Check for updates

Received: 7 December 2021 | Revised: 22 April 2022 | Accepted: 11 May 2022 | Published on: 12 June 2022

DOI: 10.1002/mrm.29320

RESEARCH ARTICLE

Magnetic Resonance in Medicine

Comparison of inversion methods in MR elastography: An open-access pipeline for processing multifrequency shear-wave data and demonstration in a phantom, human kidneys, and brain

Tom Meyer[1] | **Stephan Marticorena Garcia**[1] | **Heiko Tzschätzsch**[1] | **Helge Herthum**[2] | **Mehrgan Shahryari**[1] | **Lisa Stencel**[1] | **Jürgen Braun**[2] | **Prateek Kalra**[3,4] | **Arunark Kolipaka**[3,4] | **Ingolf Sack**[1]

[1]Department of Radiology, Charité – Universitätsmedizin Berlin, Berlin, Germany

[2]Institute of Medical Informatics, Charité – Universitätsmedizin Berlin, Berlin, Germany

[3]Department of Biomedical Engineering, The Ohio State University, Columbus, Ohio, USA

[4]Department of Radiology, The Ohio State University Wexner Medical Center, Columbus, Ohio, USA

Correspondence
Ingolf Sack, Department of Radiology, Charité – Universitätsmedizin Berlin, Charitéplatz 1, 10117 Berlin, Germany.
Email: ingolf.sack@charite.de

Funding information
German Research Foundation, Grant/Award Number: GRK2260 BIOQIC, SFB1340

Purpose: Magnetic resonance elastography (MRE) maps the viscoelastic properties of soft tissues for diagnostic purposes. However, different MRE inversion methods yield different results, which hinder comparison of values, standardization, and establishment of quantitative MRE markers. Here, we introduce an expandable, open-access, webserver-based platform that offers multiple inversion techniques for multifrequency, 3D MRE data.

Methods: The platform comprises a data repository and standard MRE inversion methods including local frequency estimation (LFE), direct-inversion based multifrequency dual elasto-visco (MDEV) inversion, and wavenumber-based (k-) MDEV. The use of the platform is demonstrated in phantom data and in vivo multifrequency MRE data of the kidneys and brains of healthy volunteers.

Results: Detailed maps of stiffness were generated by all inversion methods showing similar detail of anatomy. Specifically, the inner renal cortex had higher shear wave speed (SWS) than renal medulla and outer cortex without lateral differences. k-MDEV yielded higher SWS values than MDEV or LFE (full kidney/brain k-MDEV: $2.71 \pm 0.19/1.45 \pm 0.14$ m/s, MDEV: $2.14 \pm 0.16/0.99 \pm 0.11$ m/s, LFE: $2.12 \pm 0.15/0.89 \pm 0.06$ m/s).

Conclusion: The freely accessible platform supports the comparison of MRE results obtained with different inversion methods, filter thresholds, or excitation frequencies, promoting reproducibility in MRE across community-developed methods.

KEYWORDS
direct inversion, local frequency estimation, MRE, multifrequency magnetic resonance elastography, quantitative imaging biomarkers, viscoelasticity

This is an open access article under the terms of the Creative Commons Attribution-NonCommercial-NoDerivs License, which permits use and distribution in any medium, provided the original work is properly cited, the use is non-commercial and no modifications or adaptations are made.
© 2022 The Authors. *Magnetic Resonance in Medicine* published by Wiley Periodicals LLC on behalf of International Society for Magnetic Resonance in Medicine.

1 | INTRODUCTION

Magnetic resonance elastography (MRE)[1] is an established technique for staging liver fibrosis[2] and is currently being developed for other diagnostic applications, including brain disease,[3] cardiovascular applications,[4] and tumors.[5] MRE measures tissue viscoelasticity—an intrinsic material property that can be quantified by standardized reference methods such as shear rheometry.[6] Nevertheless, different MRE methods yield different values in the same tissue, leading to inconsistent thresholds for viscoelasticity-based detection of disease. This has been identified by experts, including the Quantitative Imaging Biomarkers Alliance (QIBA)[7] and the school for biophysical quantitative imaging in clinical diagnosis (BIOQIC),[8] as a major obstacle to the standardization and establishment of quantitative elastography markers.

Factors contributing to the variability of MRE results include the use of different excitation frequencies for mechanical stimulation and different post-processing methods. Both are typically adapted to specific requirements of spatial resolution, viscoelastic heterogeneity, noise, and compression wave components.[9]

Therefore, a single, fixed processing pipeline cannot address all requirements equally well. Different solutions to the inverse problem in MRE exist, but no multi-pipeline processing platform that fosters the standardized and comparative processing of MRE data independent of the acquisition setup. We hypothesize that comparison of values, assessment of data quality, reproducibility of MRE results, and, ultimately, standardization of thresholds for quantification of disease can be critically advanced by providing an open platform where all types of raw MRE data can universally be uploaded and processed using various established inversion methods.

Here, we introduce such a platform, which, as a starting point, offers 3 independent inversion methods using fundamentally different physical approaches: direct-inversion-based multifrequency dual elasto-visco (MDEV) inversion, wavenumber-based (*k*-)MDEV, and local frequency estimation (LFE). All have pros and cons and are widely used for MRE throughout the body. We will also demonstrate the adaptation of a processing pipeline to the criteria of different regions and organs. Therefore, we use *k*-MDEV with different filters in the human abdomen and brain. Although the abdomen suffers from enhanced shear wave attenuation, the brain is particularly reverberant and has numerous solid–fluid interfaces that pose a challenge for temporal–spatial filters such as those used in *k*-MDEV.[10] To specify the fidelity of each pipeline in resolving anatomic detail of stiffness, we analyze phantom data and a larger set of prospectively acquired in vivo multifrequency MRE data of healthy human kidneys. We chose the kidney for 3 reasons: (1) kidneys show significant heterogeneity of viscoelasticity requiring relatively high spatial resolution to depict regional differences; (2) 2 kidneys with similar properties are scanned simultaneously and can be used as internal reference for data consistency; and (3) the kidney is understudied by elastography because of its shielded location, despite an urgent clinical need for stiffness-based imaging markers in renal disease.

Collectively, our aims are, first, to introduce an open-access multi-pipeline MRE processing platform and, second, to use it for advanced quantitative MRE in the human kidney, addressing multifrequency wave data, motion correction, and regional differences.

2 | METHODS

2.1 | Subjects

The study was approved by our ethics committee and healthy volunteers were investigated after written informed consent was obtained. Twenty-three healthy volunteers were prospectively enrolled for the kidney examinations (10 women, mean age, 35 ± 11 years, age range, 21-53 years), whereas the brains of 3 subjects (1 women, 51, 47, and 57 years old) were scanned for cerebral MRE data processing.

2.2 | Phantom data

For validation, we used repository phantom data published in Papazoglou et al[11] and used in the literature for validation purposes.[10,12] The phantom was made of agar-based Wirogel (Bego, Bremen, Germany) with 4 parallel cylindrical inclusions of 11-mm diameter. Matrix and 4 inclusions were tailored to values of the magnitude shear modulus (|G*|) of 10.1 (matrix), 35.3 (inclusion 1), 4.9 (inclusion 2), 5.6 (inclusion 3), and 14.4 kPa (inclusion 4) with almost no dispersion as shown by shear rheometry within 10 to 100 Hz frequency range and corresponding parameter fits based on the spring-pot model.[11] Henceforth, phantom values obtained with different processing pipelines were averaged over all MRE frequencies (30-100 Hz, 10 Hz increments) and in-plane wave components. The out-of-plane component was not used for post processing for the following reasons: first, this component had ~3 times higher amplitudes than the in-plane components because of the dominant vibration direction of the actuator along the out-of-plane direction. This overshoot combined with relative short wavelengths

15222594, 2022, 4, Downloaded from https://onlinelibrary.wiley.com/doi/10.1002/mrm.29320 by Charite-Universitätsmedizin, Wiley Online Library on [28/03/2025]. See the Terms and Conditions (https://onlinelibrary.wiley.com/terms-and-conditions) on Wiley Online Library for rules of use; OA articles are governed by the applicable Creative Commons License

at higher frequencies affects pre-smoothing applied in abdominal *k*-MDEV as demonstrated in the Supporting Information S1. Second, because it dominated the weaker in-plane components, mixing of multicomponent information was less effective when the through-plane component was included. Therefore, the remaining 2 components reflected a more realistic in vivo scenario in terms of shared intensities and wave amplitudes.

2.3 | Multifrequency MRE in the kidney

MRE was performed on a 1.5 T MRI scanner (Magnetom Sonata, Siemens, Erlangen, Germany) using a 12-channel phased-array surface coil as described in Lang et al.[13] Briefly, all subjects were examined in supine position using 2 posterior actuators placed underneath each kidney and powered by compressed air (0.6 bar) pulses of 40, 50, 60, and 70 Hz frequency. Full wavefields were acquired in 11 contiguous paracoronal slices using a single-shot, spin-echo planar imaging sequence. Other imaging parameters were: $256 \times 256\,\text{mm}^2$ field-of-view, $2.46 \times 2.46 \times 2.5\,\text{mm}^3$ voxel size, 1200 ms repetition time, 55 ms echo time; parallel imaging with factor-2 acceleration, 25 mT/m MEG-amplitude (first moment nulling), 48.45 Hz, and 52.41 Hz MEG-frequency for vibration frequencies ≤60 Hz and 70 Hz, respectively. Total imaging time was 4 min with subjects breathing freely.

2.4 | Multifrequency MRE in the brain

Cerebral MRE was performed on a 1.5 T MRI scanner (Magnetom Aera, Siemens, Erlangen, Germany) using a 16-channel head coil. The brains were scanned with the same sequence as used in the kidney however, with 7 frequencies of 20, 25, 30, 35, 40, 45, and 50 Hz, which were induced by 2 compressed-air actuators placed underneath the head. Imaging parameters were: 30 transversal slices, $192 \times 156\,\text{mm}^2$ field-of-view, $2.0 \times 2.0 \times 2.0\,\text{mm}^3$ voxel size, 4540 ms repetition time, 88 ms echo time, 30 mT/m MEG-amplitude (first moment nulling), 27.26 Hz, 29.97 Hz, 33.68 Hz, and 54.58 Hz MEG-frequency for vibration frequencies ≤35 Hz, 40 Hz, 45 Hz, and 50 Hz, respectively. Total imaging time including 7 frequencies was 12:51 min.

2.5 | Server architecture

The MRE processing platform (https://bioqic-apps.charite.de/) was implemented as a Java web application. A diagram of the server architecture is presented in Figure 1. The web interface guides the user through the pipeline and provides explanations for available options. The Java application handles downloads and uploads of imaging data and executes compiled MATLAB scripts for data processing (The MathWorks, Natick, MA). On data upload, a MATLAB script imports the data, sorts the image data, and extracts the meta-information required for MRE processing. The following standard data formats are currently supported: real-valued DICOM (stack of 2D image slices or 3D multi frame, all common MRI system vendors are supported), real valued Nifti (4D) and real-, or complex-valued MATLAB (up to 6D, version 6 and beyond). The data should include raw MRE magnitude and phase images, which are 3D in space and ordered along the time steps over a vibration period (4th dimension). A 5th dimension is introduced by the field components along the Cartesian axes of the MRI scanner whereby their order and direction are unimportant for the pipelines evaluated in this study. A 6th dimension can be added when the MRE data were acquired with different mechanical excitation frequencies. Although the import function extracts as much as possible meta information from the data headers, all relevant parameters including voxel sizes, slice number, frequencies, and order of the image stacks can be adapted manually through the web interface. Several processing pipelines including LFE, MDEV, and *k*-MDEV can then be parameterized with presets for abdominal and cerebral MRE or by manually specifying optimized data-specific parameter settings including automated motion correction. After successful processing, the results can be downloaded in the same formats as specified above (DICOM, Nifti, and MATLAB). Communication between the web interface and the web server and file transfer is encrypted using HTTPS. The web interface uses the JavaScript-based DICOM viewer Papaya to display MRE maps. All data are automatically deleted after logging off or a 60-min time-out. A MySQL database was used for user administration.

2.6 | Inversion methods: LFE, MDEV, and k-MDEV

MDEV inversion is an approach to Helmholtz ("direct") inversion based on the magnitude formulation of the complex-valued shear wave equation providing |G*|, the magnitude of the shear modulus G* in kPa. In addition, rotation of the complex displacement vector by the 2D-Laplacian is solved for φ, the loss angle.[11] Before inversion, numerator and denominator of the inversion equation were slice-wise summed up over all wave components and frequencies according to Streitberger et al.[14] *k*-MDEV analyzes the phase-gradient of plane waves by

15222594, 2022, 4, Downloaded from https://onlinelibrary.wiley.com/doi/10.1002/mrm.29320 by Charite-Universitätsmedizin, Wiley Online Library on [28/03/2025]. See the Terms and Conditions (https://onlinelibrary.wiley.com/terms-and-conditions) on Wiley Online Library for rules of use; OA articles are governed by the applicable Creative Commons License

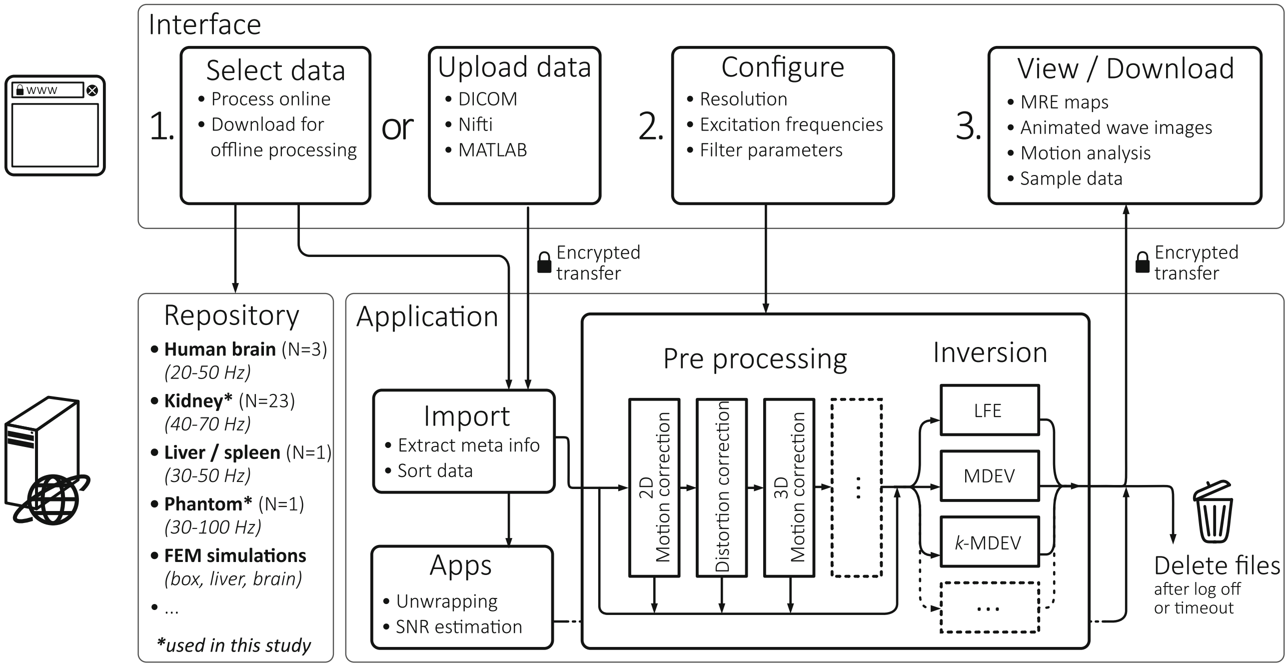

FIGURE 1 Architecture of the proposed MRE data processing server including data repository. The server is publicly accessible at https://bioqic-apps.charite.de. LFE, local frequency estimation; MDEV, multifrequency dual elasto-visco inversion; *k*-MDEV, wavenumber-based MDEV

2D-first-order derivatives, which are more noise robust than second-order derivative inversions. Waves are decomposed into plane-waves using directional filters[15] followed by extraction of complex-valued wave numbers, from which shear-wave speed (SWS in m/s, related to stiffness) and wave penetration rate (a in m/s, related to inverse wave attenuation) are obtained by inversion. Before inversion, numerator and denominator of the inversion equation were slice-wise averaged over all wave components, frequencies, and wave directions in an either unweighted (for brain) or weighted fashion (for abdomen) according to Tzschätzsch et al[12] and specified in Table 1. LFE exploits 6 pairs of lognormal filters spaced an octave apart; the magnitude of the ratio between 2 lognormal quadrature filters used in LFE provides a narrow-band estimate of the local frequency, from which tissue stiffness is spatially derived. Therefore, applied to 8 directionally filtered plane waves along with 4th-order Butterworth bandpass filer, LFE can, in principle, recover SWS similar to *k*-MDEV; however, we used LFE as the reference for commercial MRE. Therefore, an apparent stiffness parameter was obtained ($SWS^2\rho$ with ρ denoting unit mass density of 1 kg/L) after calculating a weighted sum of individual SWS^2 maps of all wave components, frequencies, and directions based on their first harmonic amplitude.[16] Comparison of values from all 3 methods was done based on SWS. All filter parameters and default settings of LFE, MDEV, and *k*-MDEV for both abdominal and cerebral applications are given in Table 1.

2.7 | Statistical analysis

Data were processed after 2D motion correction[17,18] as explained in the Supporting Information S1. Regions of interest (ROIs) of the kidney were manually drawn for the medulla, inner- and outer cortex based on multislice MRE magnitude images. Group analysis for motion correction and pairwise group-analysis between ROIs and inversion methods was performed using one-way ANOVA for repeated measures with Bonferroni correction and with Tukey's test for post-hoc analysis. Brain data were analyzed by image registration based on the MRE magnitude images using elastix with b-spline transformation and advanced Mattes mutual information as similarity metric.[19] Full brain SWS values were averaged across subjects. SNR of phantom data was analyzed based on the blind noise estimation method of Donoho et al.[20] Displacement SNR, strain SNR (octahedral shear strain)[21] and Laplacian SNR can be found online and used for any MRI data including MRE phase images. A more detailed description is given in Bertalan et al.[22] We applied all 3 SNR estimators to our phantom data, including all field components and frequencies excluding the through-plane derivative components for strain and Laplacian SNR, effectively yielding 2D strain SNR measurements. All statistical analyses were performed in R (version 4.0.3, R-Foundation) and $P < 0.05$ was considered significant. All data are displayed as mean ± standard deviation.

15222594, 2022, 4, Downloaded from https://onlinelibrary.wiley.com/doi/10.1002/mrm.29320 by Charite-Universitätsmedizin, Wiley Online Library on [28/03/2025]. See the Terms and Conditions (https://onlinelibrary.wiley.com/terms-and-conditions) on Wiley Online Library for rules of use; OA articles are governed by the applicable Creative Commons License

TABLE 1 Parameter setting for the inversion methods used in this study

Inversion method	Output parameter(s)	Pre-smoothing	Unwrapping method	Bandpass	Filter banks	Multifrequency averaging
k-MDEV abdomen (phase gradient)	Wave speed (SWS) in m/s Wave penetration rate (a) in m/s	Gaussian (σ = 2.75 mm)	Laplacian[a]	Linear highpass in k-space, no extra lowpass	8 directional-radial	Mean weighted wavenumbers with total wave amplitude to the power of 4
k-MDEV brain (phase gradient)	Wave speed (SWS) in m/s Wave penetration rate (a) in m/s	—	Laplacian[a]	Butterworth of order 3 with 15 1/m and 230 1/m upper and lower thresholds	8 directional-radial	Mean wavenumbers
MDEV (direct Helmholtz inversion)	Magnitude shear modulus $\|G^*\|$ in Pa, loss angle (φ) in rad	Gaussian (σ = 0.65 pixel size)	Gradient[b]	Highpass: gradient kernel (symmetric, 3 pixels) Lowpass: Butterworth (order 3, threshold 50/m)	—	Mean $\|G^*\|$ and φ
LFE (filtered k-space)	Apparent stiffness in Pa ($SWS^2\rho$)	-	Laplacian[a]	Butterworth bandpass (order [3, 3] threshold [4, 40]/m)	8 directional 6 pairs log-normal	Mean G′

[a]Available at https://bioqic-apps.charite.de, MATLAB code can be found in the appendix of Dittman et al.[41]
[b]According to Equation 12 in Papazoglou et al.[42]

3 | RESULTS

3.1 | Phantom analysis

Figure 2 shows the ground truth and results for phantom data using LFE, MDEV, and *k*-MDEV (abdomen) and *k*-MDEV (brain). Although all methods agreed with ground truth for matrix and softer inclusions, there was larger disparity for stiff inclusions. Specifically, none of the methods correctly recovered SWS values of the stiffest inclusion (1). Although only *k*-MDEV (abdomen) showed that inclusion 1 was stiffer than matrix and other inclusions and yielded a significant correlation between recovered stiffness values and ground truth (R = 0.9, $P < 0.05$), the other inversion methods slightly better reproduced inclusion sizes and boundaries. LFE provided the smoothest matrix contrast with least spurious variations and boundary effects of all 3 methods given that matrix stiffness in this phantom was uniform. Quantitative results are summarized in Table 2.

3.2 | In vivo kidney analysis

A full set of wave field images at 4 excitation frequencies in a paracoronal slice through the kidneys of a volunteer is presented in the Supporting Information S1.

The effect of motion correction was illustrated in Supporting Information S1 for *k*-MDEV inversion, which provided the highest contrast at tissue boundaries; however, similar results were obtained with MDEV and LFE. Greater sharpness of renal boundaries was apparent after slice-wise 2D-motion correction. Adding through-plane motion correction (3D) to 2D-corrected wave data appeared not to further improve sharpness of kidney anatomy in SWS maps. Interestingly, averaged SWS values of the full parenchyma were uninfluenced by motion correction (all $P > 0.05$) corroborating previous findings.[17] Nevertheless, given the clear improvement in image sharpness at little cost, 2D-motion correction was added as a preprocessing module to all 3 methods.

Representative slices of kidney SWS obtained by LFE, MDEV, and *k*-MDEV were shown in Figure 3A. *k*-MDEV SWS values were higher than MDEV and LFE values (full-kidney SWS: 2.71 ± 0.19 m/s [*k*-MDEV], 2.14 ± 0.16 m/s [MDEV], 2.12 ± 0.15 m/s [LFE], each $P < 0.001$). Additionally, *k*-MDEV visualized renal substructures in greater detail than the other 2 methods. Consistently, all 3 methods showed the inner renal cortex to be stiffer (*k*-MDEV: 3.3 ± 0.3 m/s, MDEV: 2.4 ± 0.2 m/s, LFE: 2.0 ± 0.4 m/s) than medulla (*k*-MDEV: 2.7 ± 0.2 m/s, MDEV: 2.3 ± 0.2 m/s, LFE: 1.9 ± 0.3 m/s), and outer cortex (*k*-MDEV: 2.5 ± 0.3 m/s, MDEV: 1.9 ± 0.1 m/s,

15222594, 2022, 4, Downloaded from https://onlinelibrary.wiley.com/doi/10.1002/mrm.29320 by Charite-Universitätsmedizin, Wiley Online Library on [28/03/2025]. See the Terms and Conditions (https://onlinelibrary.wiley.com/terms-and-conditions) on Wiley Online Library for rules of use; OA articles are governed by the applicable Creative Commons License

15222594, 2022, 4, Downloaded from https://onlinelibrary.wiley.com/doi/10.1002/mrm.29320 by Charite-Universitätsmedizin, Wiley Online Library on [28/03/2025]. See the Terms and Conditions (https://onlinelibrary.wiley.com/terms-and-conditions) on Wiley Online Library for rules of use; OA articles are governed by the applicable Creative Commons License

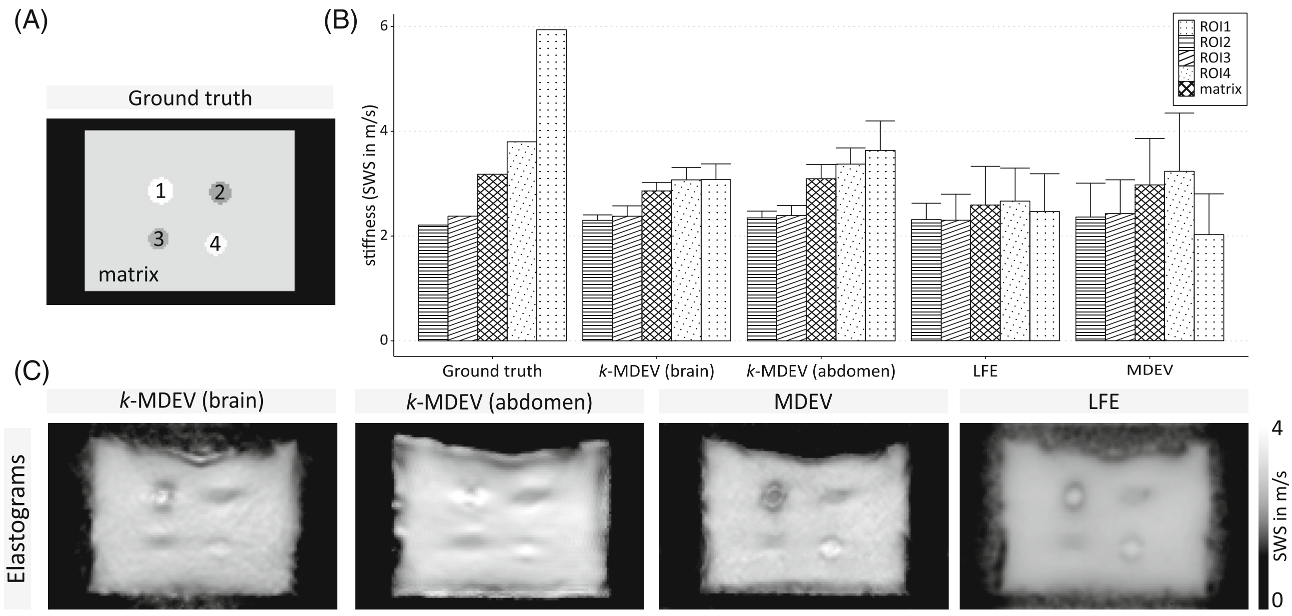

FIGURE 2 Phantom results. (A) Ground truth shear-wave speed (SWS) map. (B) Mean SWS results with standard deviation of the regions shown in (A). (C) SWS maps obtained with LFE, MDEV and *k*-MDEV (for both brain and abdominal organs)

TABLE 2 Phantom values obtained by the inversion methods used in this study and SNR

	Shear wave speed in m/s					**SNR in dB**		
	Ground truth	***k*-MDEV (brain)**	***k*-MDEV (abdomen)**	**MDEV**	**LFE**	**Displacement**	**Strain**	**Laplacian**
Matrix	3.2	2.9 (0.2)	3.1 (0.3)	3.0 (0.9)	2.6 (0.7)	28.8 (2.4)	17.0 (3.9)	−5.6 (0.5)
Incl. 1	5.9	3.1 (0.3)	3.6 (0.6)	2.0 (0.8)	2.5 (0.7)	17.6 (5.4)	0.7 (2.1)	−6.2 (0.4)
Incl. 2	2.2	2.3 (0.1)	2.3 (0.1)	2.4 (0.6)	2.3 (0.3)	30.5 (3.5)	21.8 (3.8)	−4.14 (1.6)
Incl. 3	2.4	2.4 (0.2)	2.4 (0.1)	2.4 (0.6)	2.3 (0.5)	28.4 (4.6)	17.6 (4.4)	−4.3 (1.1)
Incl. 4	3.8	3.1 (0.2)	3.4 (0.3)	3.2 (1.1)	2.7 (0.6)	26.4 (4.5)	12.9 (6.2)	−5.5 (0.5)
Correlation (*R*) with ground truth		0.8 ($P > 0.05$)	0.9 ($P < 0.05$)	−0.3 ($P > 0.05$)	0.4 ($P > 0.05$)			

Mean values with standard deviations in brackets. Phantom data, inversion pipelines, and SNR estimation tools are available at https://bioqic-apps.charite.de.

LFE: 1.8 ± 0.2 m/s, all $P < 0.05$) without lateral differences (all $P > 0.05$). Group values for all volunteers were summarized in Figure 3B.

3.3 | In vivo brain analysis

Figure 4 shows group-averaged SWS maps of the human brain obtained with LFE, MDEV, and *k*-MDEV, the latter adapted for cerebral MRE according to Table 1. Anatomic detail such as stiff putamen and white matter compared with relatively soft cortical gray matter are well visible with all 3 methods. As in the kidney, *k*-MDEV yielded higher SWS values than MDEV or LFE (full brain *k*-MDEV: 1.45 ± 0.14 m/s, MDEV: 0.99 ± 0.11 m/s, LFE: 0.89 ± 0.06 m/s) consistent to Herthum et al.[10] LFE showed least variance over full brain tissue similar to phantom results.

4 | DISCUSSION

Here, we presented an open-access, processing platform for multifrequency, 3D MRE data offering comparative processing using multiple inversion methods. Beyond wave inversion with standardized pipelines of LFE, MDEV,

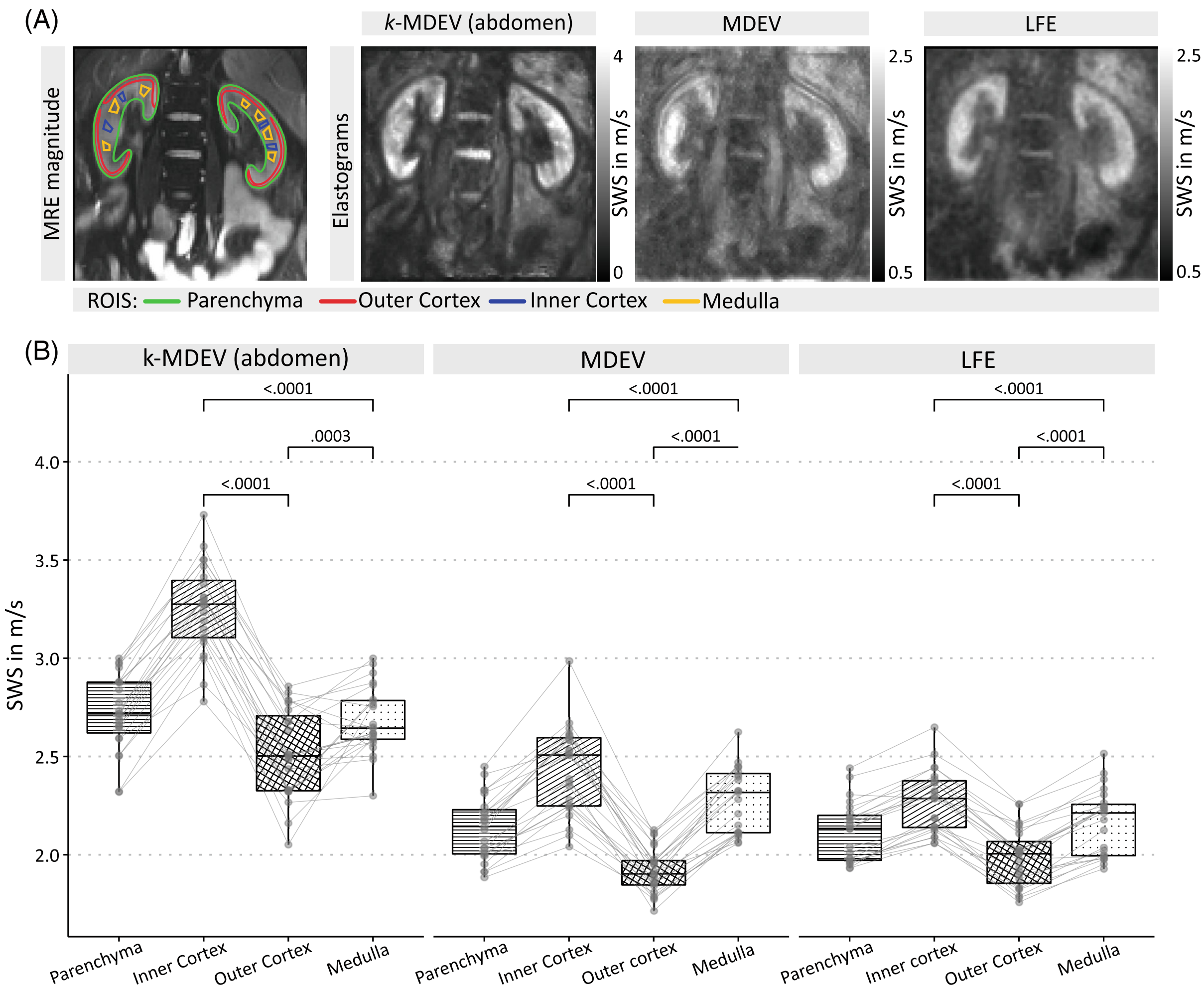

FIGURE 3 (A) Comparison of SWS (shear-wave speed) maps of multifrequency MRE of the kidney in a healthy volunteer obtained by LFE (local frequency estimation), MDEV (multifrequency dual elasto-visco inversion), and *k*-MDEV (wavenumber-based MDEV) with both gray scale (unit axes). Region of interest (ROI) selection is illustrated by solid colored lines in MRE magnitude images. (B) Group statistical plots of regional SWS (shear-wave speed) values of the kidney (averaged over the right and left kidney in each volunteer) as obtained by 3 different processing pipelines implemented at https://bioqic-apps.charite.de. LFE, local frequency estimation; MDEV, multifrequency dual elasto-visco inversion; *k*-MDEV, wavenumber-based MDEV

and *k*-MDEV, the platform incorporates modular preprocessing blocks such as 2D- and 3D-motion correction[17] and distortion correction[23] as well as wave analysis options including SNR analysis. These modules can be expanded by more sophisticated phase unwrapping,[24] denoising,[25] SNR analysis,[21] and dejittering,[26] which might also be favorable for other established inversion algorithms such as nonlinear inversion,[27] anisotropic inversion,[28–30] wave-fitting approaches,[31] or divergence free finite element reconstruction.[32] These community-wide established methods can easily be implemented on our server, provided that they support time efficient data processing within less than a minute for a 3D set of single-frequency MRE data. The wide range of supported data formats, filter settings, and inversion options including pre- and post-processing modules that can be selected and controlled via structured web interfaces ensures high usability of the platform.

An important feature of this platform is the repository of MRE data, to which the community has contributed.[26,33] The stored data can either be directly processed or downloaded for offline use to promote fair comparison of pipelines and to allow researchers to reproduce the detail resolution, consistency, and accuracy of published methods. Currently, simulated brain and liver data and sets of multifrequency wave field data of the phantom presented here, which was used as reference in multiple studies, as well as in vivo data of healthy volunteers of the brain, the liver, and the kidney datasets presented here are available. This rich database includes 60 Hz frequency and wave components that are typically exploited in clinical MRE and, therefore, permits extraction of subsets of data

15222594, 2022, 4, Downloaded from https://onlinelibrary.wiley.com/doi/10.1002/mrm.29320 by Charite-Universitätsmedizin, Wiley Online Library on [28/03/2025]. See the Terms and Conditions (https://onlinelibrary.wiley.com/terms-and-conditions) on Wiley Online Library for rules of use; OA articles are governed by the applicable Creative Commons License

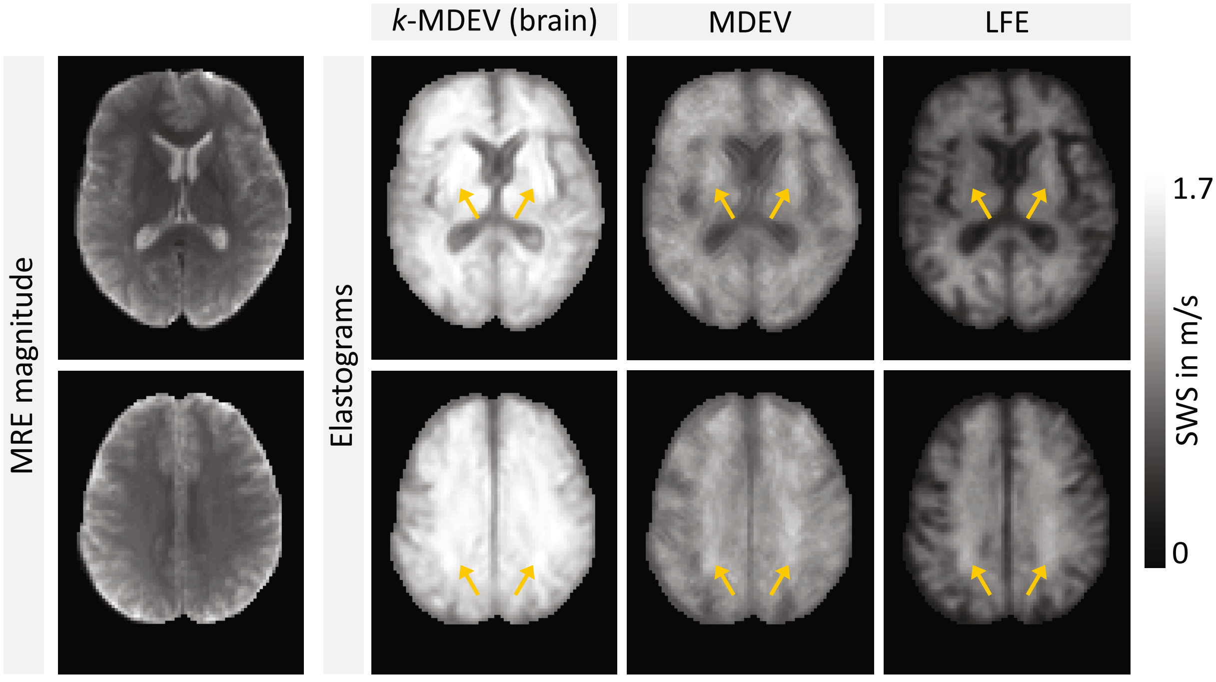

FIGURE 4 Two slices of registered and group-averaged shear-wave speed (SWS) maps of the brains of 3 healthy volunteers obtained with LFE, MDEV, and k-KMDEV. All 3 methods consistently show stiffer properties in regions of deep gray matter (putamen) and white matter (yellow arrows)

for comparison with clinical data. More data from other MRE sequences or simulation studies are welcome.

Beyond presenting novel MRE processing tools, this study is the first comparative analysis of renal stiffness encompassing multiple inversion pipelines with motion-corrected multifrequency wave data. Our results are consistent with renal stiffness measured by tomoelastography (SWS = 2.34 ± 0.15 m/s,[13] 2.40 ± 0.17 m/s, based on *k*-MDEV inversion)[34] and single-frequency MRE (60 Hz, 1.82 ± 0.54 m/s based on LFE).[16] Although tomoelastography consistently showed that the inner cortex was stiffer than medulla and outer cortex (2.92 ± 0.25 m/s, 2.41 ± 0.13 m/s, 2.16 ± 0.18 m/s),[34] previous work based on LFE did not resolve inner and outer cortex,[16] but showed that averaged cortex tissue is softer than medulla (3.63 ± 1.25 kPa vs. 4.77 ± 2.03 kPa).[35] Remarkably, no inversion method revealed lateral differences in kidney values, demonstrating the consistency of renal MRE. This agrees with studies, which indicated that lateral differences of renal stiffness may result from arbitrary statistical fluctuations[36,37] and that differences between the right and left kidney as observed by ultrasound shear wave elastography and MRE should be taken with caution.[16,38] The significantly higher values obtained with *k*-MDEV and MDEV are expected from analysis of noise responses of first- and second-order derivative kernels invoked by *k*-MDEV and MDEV, respectively.[39] Although noise at lower wave numbers (k) generally decreases stiffness estimates, *k*-MDEV outperforms other inversion techniques in the presence of noise at $k < 1$ as demonstrated in Tzschätzsch et al.[12] Similarly, LFE is also robust to noise as the inversion is performed in k-space compared to image domain in other inversion strategies.[15]

Our phantom data highlight the strengths and weaknesses of different inversion pipelines and show that a universal solution to all inverse problems in MRE may not be feasible. For example, inclusion 4 combines properties that make wavenumber estimation in MRE difficult. Here, strain SNR was below the threshold used in other MRE applications (e.g., 3 for nonlinear inversions or 1.17 in cardiac MRE).[21,40] Gaussian pre-smoothing implemented in *k*-MDEV (abdomen) apparently helps to reduce the dispersion-by-inversion bias, which is known to lead to underestimated stiffness values for long and noisy waves.[39] Based on spatial fidelity, it could be concluded that LFE is best for the stiffness of the matrix, MDEV for that of inclusion 4, whereas *k*-MDEV (brain) best represents inclusions 2 to 4. However, *k*-MDEV (abdomen) is recommended considering the overall correlation of stiffness values with ground truth. It should be noted that for the kidney and brain the ground truth of mechanical details in heterogeneous tissue is unknown. Therefore, the anatomic details revealed by the presented pipelines in vivo need to be validated in future studies.

15222594, 2022, 4, Downloaded from https://onlinelibrary.wiley.com/doi/10.1002/mrm.29320 by Charite-Universitätsmedizin, Wiley Online Library on [28/03/2025]. See the Terms and Conditions (https://onlinelibrary.wiley.com/terms-and-conditions) on Wiley Online Library for rules of use; OA articles are governed by the applicable Creative Commons License

Our study is limited by not presenting the full functionality, range of parameter settings, modules, and possible targets of our platform. For consistency, we focused on prospectively acquired kidney and brain data using default parameter settings as published elsewhere in individual studies.[34] We also focused on stiffness, which is the primary parameter in elastography, ignoring viscosity values provided by *k*-MDEV and MDEV inversion. Viscous properties are extremely rich in information regarding microstructural interactions in soft tissues. However, viscosity denotes different material properties including wave attenuation (as given by the a-parameter in *k*-MDEV) or the loss angle (as given by the ϕ-parameter in MDEV). Therefore, viscous parameters must be compared based on viscoelastic models, whereas the stiffness of elastic materials is clearly defined. The convertibility, comparability, and consistency of viscous parameters are another strong argument for processing MRE data with an open-access platform that offers standardized methods. Although these methods are currently implemented in 2D, their extensions to 3D have already been used in studies of the brain and abdominal organs[41] and will be made available on the proposed platform. However, as discussed for our 2D pipelines, there is no universal method, and 3D comes at the cost of scan time for larger volume data. Three-dimensional Fourier filters (in *k*-MDEV and LFE) and 3D finite difference operators (in MDEV) are impoverished by the small number of (frequently thick) slices that can be acquired with current MRE protocols tailored for abdominal imaging. Many abdominal MRE studies are still performed based on 2D inversions, even when 3D wave data are acquired. The suitability of 2D inversions is probably because of the fact that the coverage of regions in the center of abdominal organs apparently satisfies the geometric constraints of 2D wave processing. The proposed platform can promote a fair comparison between 2D and 3D MRE data processing in the future. In this context, it would even be possible to implement a trained data quality and consistency check that recommends the most appropriate processing pipeline based on some relevant parameters such as SNR, number of wavefield components, image slices, frequencies, and phase wraps as well as wave penetration.

In summary, we addressed the well-known lack of comparability of MRE results by introducing an expandable, easy-to-use, open-access platform that offers inversion techniques for multifrequency, MRE including LFE, MDEV and *k*-MDEV inversion. We used the platform in phantom data and, in vivo, in the kidneys and brains of healthy subjects. In the kidneys we found that, after motion correction, all methods consistently showed regional differences and similar values for both kidneys. The platform might foster the development of quantitative imaging biomarkers related to tissue viscoelasticity by facilitating analysis of effects of filter thresholds, spatial resolution, motion, and frequency dispersion on MRE results.

ACKNOWLEDGMENTS

Stephan Marticorena Garcia received funding from the German Research Foundation (project number 467843609). Support of the German Research Foundation (GRK2260 BIOQIC, SFB1340) is gratefully acknowledged.

ORCID

Tom Meyer https://orcid.org/0000-0002-2171-6791
Helge Herthum https://orcid.org/0000-0001-6494-0833
Mehrgan Shahryari https://orcid.org/0000-0002-3981-1711
Jürgen Braun https://orcid.org/0000-0001-5183-7546
Ingolf Sack https://orcid.org/0000-0003-2460-1444

REFERENCES

1. Muthupillai R, Ehman RL. Magnetic resonance elastography. *Nature Med*. 1996;2:601-603.
2. Kennedy P, Wagner M, Castera L, et al. Quantitative elastography methods in liver disease: current evidence and future directions. *Radiology*. 2018;286:738-763.
3. Hiscox LV, Johnson CL, Barnhill E, et al. Magnetic resonance elastography (MRE) of the human brain: technique, findings and clinical applications. *Phys Med Biol*. 2016;61:R401-R437.
4. Khan S, Fakhouri F, Majeed W, Kolipaka A. Cardiovascular magnetic resonance elastography: a review. *NMR Biomed*. 2018;31:e3853.
5. Garteiser P, Doblas S, Daire JL, et al. MR elastography of liver tumours: value of viscoelastic properties for tumour characterisation. *Eur Radiol*. 2012;22:2169-2177.
6. Manduca A, Bayly PJ, Ehman RL, et al. MR elastography: principles, guidelines, and terminology. *Magn Reson Med*. 2021;85:2377-2390.
7. Palmeri ML, Milkowski A, Barr R, et al. Radiological Society of North America/quantitative imaging biomarker Alliance shear wave speed bias quantification in elastic and viscoelastic phantoms. *J Ultrasound Med*. 2021;40:569-581.
8. Sack I. Forschungsförderung – BIOQIC – Neue Generation von Bildgebungsspezialisten. *Rofo*. 2017;188:86.
9. Hirsch S, Braun J, Sack I. *Magnetic Resonance Elastography: Physical Background and Medical Applications*. Wiley-VCH; 2017.
10. Herthum H, Hetzer S, Scheel M, et al. In vivo stiffness of multiple sclerosis lesions is similar to that of normal-appearing white matter. *Acta Biomater*. 2021;138:410-421.
11. Papazoglou S, Hirsch S, Braun J, Sack I. Multifrequency inversion in magnetic resonance elastography. *Phys Med Biol*. 2012;57:2329-2346.

15222594, 2022, 4, Downloaded from https://onlinelibrary.wiley.com/doi/10.1002/mrm.29320 by Charite-Universitätsmedizin, Wiley Online Library on [28/03/2025]. See the Terms and Conditions (https://onlinelibrary.wiley.com/terms-and-conditions) on Wiley Online Library for rules of use; OA articles are governed by the applicable Creative Commons License

12. Tzschatzsch H, Guo J, Dittmann F, et al. Tomoelastography by multifrequency wave number recovery from time-harmonic propagating shear waves. *Med Image Anal*. 2016; 30:1-10.
13. Lang ST, Guo J, Bruns A, et al. Multiparametric quantitative MRI for the detection of IgA nephropathy using Tomoelastography, DWI, and BOLD imaging. *Invest Radiol*. 2019; 54:669-674.
14. Streitberger KJ, Reiss-Zimmermann M, Freimann FB, et al. High-resolution mechanical imaging of glioblastoma by multifrequency magnetic resonance elastography. *PLoS One*. 2014;9:e110588.
15. Manduca A, Lake DS, Kruse SA, Ehman RL. Spatio-temporal directional filtering for improved inversion of MR elastography images. *Med Image Anal*. 2003;7:465-473.
16. Gandhi D, Kalra P, Raterman B, Mo XK, Dong HM, Kolipaka A. Magnetic resonance elastography-derived stiffness of the kidneys and its correlation with water perfusion. *NMR Biomed*. 2020;33:e4237.
17. Shahryari M, Meyer T, Warmuth C, et al. Reduction of breathing artifacts in multifrequency magnetic resonance elastography of the abdomen. *Magn Reson Med*. 2021;85: 1962-1973.
18. Reddy BS, Chatterji BN. An FFT-based technique for translation, rotation, and scale-invariant image registration. *IEEE Trans Image Process*. 1996;5:1266-1271.
19. Klein S, Staring M, Murphy K, Viergever MA, Pluim JPW. Elastix: a toolbox for intensity-based medical image registration. *IEEE Trans Med Imaging*. 2010;29:196-205.
20. Donoho DL, Johnstone IM, Kerkyacharian G, Picard D. Wavelet shrinkage - ASYMPTOPIA. *J Roy Stat Soc Ser B*. 1995; 57:301-337.
21. McGarry MDJ, Van Houten EEW, Perrinez PR, Pattison AJ, Weaver JB, Paulsen KD. An octahedral shear strain-based measure of SNR for 3D MR elastography. *Phys Med Biol*. 2011;56:N153-N164.
22. Bertalan G, Guo J, Tzschatzsch H, et al. Fast tomoelastography of the mouse brain by multifrequency single-shot MR elastography. *Magn Reson Med*. 2019;81:2676-2687.
23. Fehlner A, Hirsch S, Weygandt M, et al. Increasing the spatial resolution and sensitivity of magnetic resonance elastography by correcting for subject motion and susceptibility-induced image distortions. *J Magn Reson Imaging*. 2017;46:134-141.
24. Barnhill E, Kennedy P, Johnson CL, Mada M, Roberts N. Real-time 4D phase unwrapping applied to magnetic resonance elastography. *Magn Reson Med*. 2015; 73:2321-2331.
25. Barnhill E, Hollis L, Sack I, et al. Nonlinear multiscale regularisation in MR elastography: towards fine feature mapping. *Med Image Anal*. 2017;35:133-145.
26. Barnhill E, Nikolova M, Ariyurek C, Dittmann F, Braun J, Sack I. Fast robust Dejitter and interslice discontinuity removal in MRI phase acquisitions: application to magnetic resonance Elastography. *IEEE Trans Med Imaging*. 2019; 38:1578-1587.
27. McGarry MD, Van Houten EE, Johnson CL, et al. Multiresolution MR elastography using nonlinear inversion. *Med Phys*. 2012;39:6388-6396.
28. Guo J, Hirsch S, Scheel M, Braun J, Sack I. Three-parameter shear wave inversion in MR elastography of incompressible transverse isotropic media: application to in vivo lower leg muscles. *Magn Reson Med*. 2016;75:1537-1545.
29. Kalra P, Raterman B, Mo X, Kolipaka A. Magnetic resonance elastography of brain: comparison between anisotropic and isotropic stiffness and its correlation to age. *Magn Reson Med*. 2019;82:671-679.
30. Babaei B, Fovargue D, Lloyd RA, et al. Magnetic resonance elastography reconstruction for anisotropic tissues. *Med Image Anal*. 2021;74:102212.
31. Baghani A, Salcudean S, Honarvar M, Sahebjavaher RS, Rohling R, Sinkus R. Travelling wave expansion: a model fitting approach to the inverse problem of elasticity reconstruction. *IEEE Trans Med Imaging*. 2011;30: 1555-1565.
32. Fovargue D, Kozerke S, Sinkus R, Nordsletten D. Robust MR elastography stiffness quantification using a localized divergence free finite element reconstruction. *Med Image Anal*. 2018;44:126-142.
33. Ariyurek C, Tasdelen B, Ider YZ, Atalar E. SNR weighting for shear wave speed reconstruction in tomoelastography. *NMR Biomed*. 2020;34:e4413.
34. Marticorena Garcia SR, Grossmann M, Bruns A, et al. Tomoelastography paired with T2* magnetic resonance imaging detects lupus nephritis with normal renal function. *Invest Radiol*. 2019;54:89-97.
35. Guven AT, Idilman IS, Cebrayilov C, et al. Evaluation of renal fibrosis in various causes of glomerulonephritis by MR elastography: a clinicopathologic comparative analysis. *Abdom Radiol (NY)*. 2022;47:288-296.
36. Low G, Owen NE, Joubert I, et al. Reliability of magnetic resonance elastography using multislice two-dimensional spin-echo echo-planar imaging (SE-EPI) and three-dimensional inversion reconstruction for assessing renal stiffness. *J Magn Reson Imaging*. 2015;42:844-850.
37. Bob F, Bota S, Sporea I, Sirli R, Petrica L, Schiller A. Kidney shear wave speed values in subjects with and without renal pathology and inter-operator reproducibility of acoustic radiation force impulse elastography (ARFI)--preliminary results. *PLoS One*. 2014;9:e113761.
38. Singh H, Panta OB, Khanal U, Ghimire RK. Renal cortical elastography: normal values and variations. *J Med Ultrasound*. 2017;25:215-220.
39. Mura J, Schrank F, Sack I. An analytical solution to the dispersion-by-inversion problem in magnetic resonance elastography. *Magn Reson Med*. 2020;84:61-71.
40. Arani A, Arunachalam SP, Chang ICY, et al. Cardiac MR elastography for quantitative assessment of elevated myocardial stiffness in cardiac amyloidosis. *J Magn Reson Imaging*. 2017;46:1361-1367.
41. Dittmann F, Hirsch S, Tzschatzsch H, Guo J, Braun J, Sack I. In vivo wideband multifrequency MR elastography of the human brain and liver. *Magn Reson Med*. 2016; 76:1116-1126.
42. Papazoglou S, Xu C, Hamhaber U, et al. Scatter-based magnetic resonance elastography. *Phys Med Biol*. 2009; 54:2229-2241.

15222594, 2022, 4, Downloaded from https://onlinelibrary.wiley.com/doi/10.1002/mrm.29320 by Charite-Universitätsmedizin, Wiley Online Library on [28/03/2025]. See the Terms and Conditions (https://onlinelibrary.wiley.com/terms-and-conditions) on Wiley Online Library for rules of use; OA articles are governed by the applicable Creative Commons License

SUPPORTING INFORMATION

Additional supporting information may be found in the online version of the article at the publisher's website.

APPENDIX S1 Supplementary Information

How to cite this article: Meyer T, Marticorena Garcia S, Tzschätzsch H, et al. Comparison of inversion methods in MR elastography: An open-access pipeline for processing multifrequency shear-wave data and demonstration in a phantom, human kidneys, and brain. *Magn Reson Med*. 2022;88:1840-1850. doi: 10.1002/mrm.29320

15222594, 2022, 4, Downloaded from https://onlinelibrary.wiley.com/doi/10.1002/mrm.29320 by Charite-Universitätsmedizin, Wiley Online Library on [28/03/2025]. See the Terms and Conditions (https://onlinelibrary.wiley.com/terms-and-conditions) on Wiley Online Library for rules of use; OA articles are governed by the applicable Creative Commons License